TEM INVESTIGATION OF NEUTRON IRRADIATED AND ELECTRON BEAM EXPOSED TUNGSTEN

W. VAN RENTERGHEM, I. UYTDENHOUWEN
Nuclear Materials Science Institute, SCK•CEN,
Boeretang 200, 2400 Mol - Belgium

ABSTRACT

Pure tungsten samples were neutron irradiated in the BR2 reactor of SCK•CEN to fluences of 1.47×10^{20} n/cm² and 4.74×10^{20} n/cm² at 300 °C under Helium atmosphere and exposed to the electron beam of the Judith I installation to simulate the effect of a plasma disruption. The effect of these treatments on the defect structure was studied with transmission electron microscopy and a method was applied to prepare a sample close to the exposed surface. In the irradiated samples the defect structure in the bulk is compared to the structure at the surface. The neutron irradiation created a large amount of a/2‹111› type dislocation loops forming dislocation rafts. The electron beam exposure induced significant annealing of the defects and almost all of the dislocation loops were removed. The number of line dislocations in that area increased as a result of the thermal stresses resulting from the electron beam exposure.

1. Introduction

The fusion of deuterium and tritium results in the formation of a helium atom and a neutron. These neutrons, which have an energy of 14.1 MeV, will interact with the reactor wall materials and affect the mechanical properties of the reactor materials. This interaction was not an issue in the existing fusion reactors, because most experiments did not use the tritium gas and even when it was used, the total amount of fusion reactions and hence the total amount of 14.1 MeV neutrons was small and the effect on the structural components was minimal. In future reactors, like ITER, DEMO, or eventually fusion power plants, the amount of neutrons will be considerably higher [1] and it must be studied which effect neutron irradiation will have on the mechanical properties of the materials that will be used. Tungsten is the main candidate for first wall and divertor materials and will face the highest degree of neutron irradiation [2]. Therefore, it's of primordial interest to study the effect of the neutron irradiation on the defect structure.

A difficulty in the study of irradiation effects is that there is no installation available, at present, that produces large amounts of such high energy neutrons. Only nuclear fission test reactors are capable of producing high neutron fluxes, but the energy of these neutrons is at most a few MeV. Moreover, the temperature at which the materials can be irradiated differs from the operating temperature in the fusion reactor.

Apart from the neutron irradiation, the first wall material will also be exposed to transient events of the plasma [3]. One of the events are disruptions during which a high amount of energy is transferred from the plasma to the reactor wall. These events do not occur very

frequently and should be avoided as much as possible because the effect on the material integrity is very strong.

In this investigation, tungsten was irradiated in the BR2 reactor of SCK•CEN to fluences of 1.47×10^{20} n/cm² and 4.74×10^{20} n/cm² at 300°C. Afterwards the samples were exposed to the electron beam in the Judith I installation of FZ. Jülich under conditions that simulate disruptions. The effect of combined neutron irradiation and electron beam exposure is studied with scanning (SEM) and transmission electron microscopy (TEM).

2. Experimental

The tungsten material studied here was obtained from a highly deformed tungsten bar provided by Plansee AG, Austria. Three discs of 10 mm diameter and 5 mm thick were produced. The surface of the discs is mechanically polished before further exposures. The three discs are labelled ref W, low dose and high dose. Sample ref W was kept as a reference. It was neither neutron irradiated nor exposed to the electron beam. The other two samples were neutron irradiated in the BR2 reactor of SCK•CEN at a temperature of 300 °C and in a helium atmosphere. The low dose sample was irradiated to a neutron fluence (E > 1 MeV) of 1.47×10^{20} n/cm². The high dose sample was irradiated to a neutron fluence (E > 1 MeV) of 4.74×10^{20} n/cm².

After neutron irradiation, both samples were exposed to the electron beam of the JUDITH I facility at FZ Jülich. They were exposed to one pulse of 5 ms on an area of 4x4 mm^2 and the absorbed power density was 0.33 GW/m². These loading conditions are representative of a plasma disruption. In Fig. 1a, the absorbed current is plotted as a function of the pulse length. The evolution of the average surface temperature was measured with a pyrometer and the result is given in Fig. 1b. The pyrometer is not sensitive to temperatures below 1100 K and therefore the temperature seems to increase only after 1.5 ms pulse length, but in reality it starts to increase from the start. It was measured that the surface temperature increased to 1520 K at the end of the pulse, after which the temperature drops to below 1100 K in 3 ms. The temperature of 1520 K is below the recrystallisation temperature but above the limit for vacancy migration. Fig. 1c shows the calculated temperature as a function of the distance to the surface. The temperature at the surface (x = 0 mm) is in good agreement with the measured temperature. As a result of the long exposure pulse, the temperature increase reaches a depth of 1.2 mm. The effect of the electron beam exposure was studied with SEM in a JEOL 6310 instrument.

a)

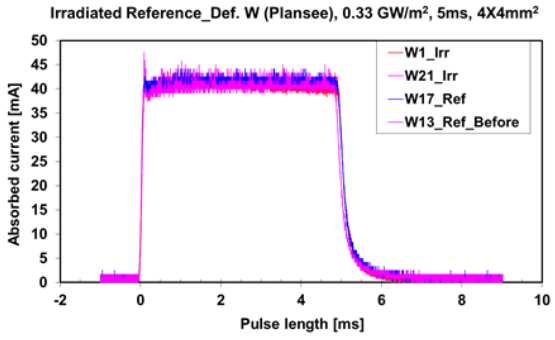

b)

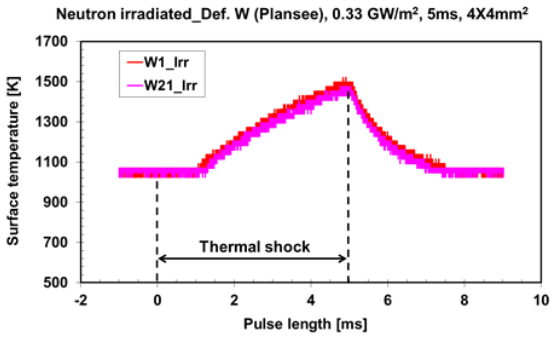

c)

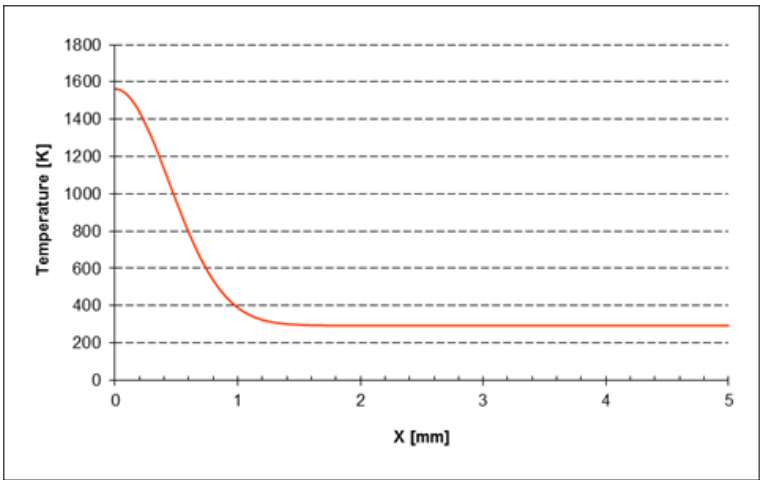

Fig. 1. Graphs showing a) the absorbed current as a function of the pulse length, b) the measured average surface temperature as a function of pulse length and c) calculated evolution of the maximal temperature as a function of the distance to the surface.

For this study, five samples were produced from the three discs. From the reference material, only a bulk sample was prepared. From the irradiated samples, one sample was prepared from the bulk and one sample was prepared close to the surface. The difficulty with the latter sample is that it needs to be prepared as close to the surface as possible. The sample preparation is schematically represented in Fig. 2. First a 1.5 mm thick disc is cut from the sample. Two laths are cut from this disc. A first lath (no. 1 in the figure) has a width of about 2 mm and contains the exposed area. The bottom part of this lath is removed by mechanical polishing on SiC paper until the thickness is reduced to 0.1 mm. A platelet was taken from the exposed part of the surface. The second lath (no. 2 in the figure) has a width of about 1 mm. This sample was flipped (top indicates the top surface from the disc) and mechanically polished from both sides to reduce the thickness to 0.1 mm. One platelet was cut off, giving the cross-section orientation.

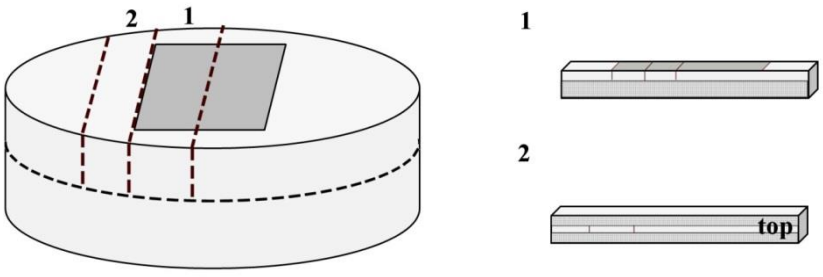

Fig. 2. Schematic representation of the sample preparation. The dark grey area was exposed to the electron beam. The dashed lines are the cutting lines and the light grey area is the material removed during polishing.

The final step of the sample preparation was electrochemical polishing using a Struers Tenupol-5 instrument . The sizes of all platelets are of the order of 1.5-2 mm. The platelets were glued on a 3 mm copper 1 mm aperture grid to be able to mount them in a TEM holder. The polishing conditions were the same for all samples. The electrolyte consisted of 1.5 wt% NaOH in water and the voltage that was applied was 20 V. All bulk samples, from the

reference material as well as the irradiated samples, were double jet polished until perforation. To prepare a sample close to the exposed surface, single jet polishing was applied in which only material from the back side of the sample is removed. However, applying only single jet polishing will rarely give good samples. As a result of the surface roughness, also the TEM transparent area will be rough and affect the measurements. Moreover, surface contamination and oxidation will not be removed, thereby obstructing the characterization of the defects induced by neutron irradiation and electron beam exposure. Therefore, the two surface exposed samples were double jet polished for 10 s, to remove the surface roughness, after which polishing was continued from the back side only until perforation. It was not determined exactly how much material was removed from the exposed side, but it's not more than a few micrometer.

All samples were investigated in a JEOL 3010 microscope operating at 300 kV. Conventional bright field, dark field and weak beam imaging was used. The local thickness was determined from convergent beam electron diffraction (CBED) patterns.

3. Results and discussion

3.1 Reference sample ref W

The grain structure obtained from the TEM investigation is shown in Fig. 3. These images reveal that the crystal grains have a sub-grain structure. The difference in orientation between part of the grains is small and they are separated by small-angle grain boundaries, but other grains have a completely different orientation and they are separated by large-angle grain boundaries. An example of both types of grain boundaries is shown in Fig. 3b. Tungsten materials with a sub-grain structure, studied previously [4,5] did not have large-angle sub-grain boundaries and also the difference in grain orientation at the low-angle grain boundaries is larger in this material. The average size of the sub-grains is 1.6 µm.

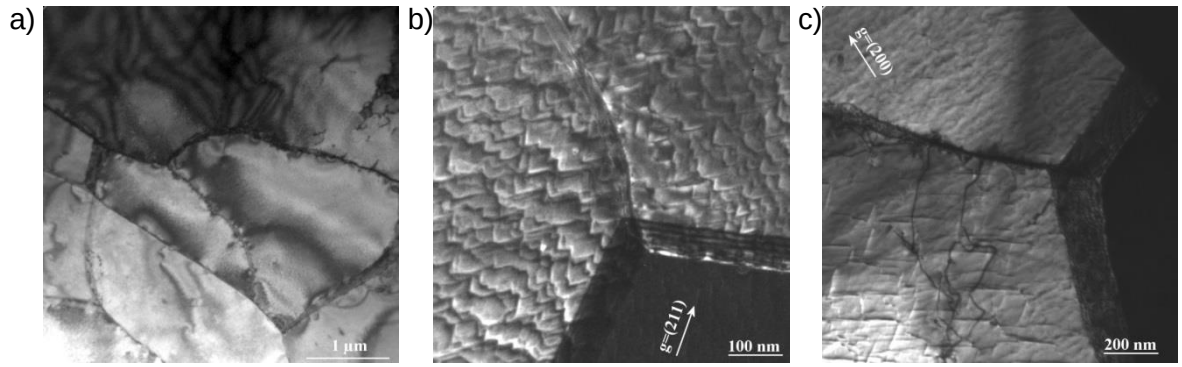

Fig. 3. a) Bright field image of the grain structure of the reference material. b) Dark field image at a triple junction of a small-angle and a large-angle grain boundary and c) dark field image a few line dislocations near the grain boundary.

Apart from the grain boundaries, very few defects are present. Most of the contrast in Fig. 3b is due to polishing effects which resulted in a stepped surface. There are no defects visible in the interior of the grain and only near the grain boundaries some line dislocations can be observed. **Error! Reference source not found.**From the verification of the extinction conditions it can be concluded that most of the dislocations are a/2‹111› type. In general the Burgers vector is also parallel to the dislocation line, which means that they are screw dislocations. A minority of the line dislocations have an a‹100› Burgers vector. These

dislocations are usually formed as a result of the interaction between two a/2‹111› type dislocations.

The observed defect structure is quite typical for a double forged and annealed tungsten material, which was not subjected to a recrystallization treatment. The stress relief annealing removes most of the defects in the grains but it doesn't remove the sub-grains as in higher temperature recrystallization treatments at 1500K or above. The larger orientation difference between the sub-grains is probably the result of the high deformation in the tungsten rod.

3.2 Low dose irradiated sample (1.47×10^{20} n/cm²)

The temperature of the neutron irradiation it too low to have an effect on the grain structure and this is confirmed in the low dose sample. Typical grains of the sample are shown in Fig. 4a. A sub-grain structure can be observed which is limited by both low-angle and high-angle grain boundaries. The average size of the sub-grains is still of the order of 2 µm. The interior of the grains is covered with a large amount of typical radiation induced defects.

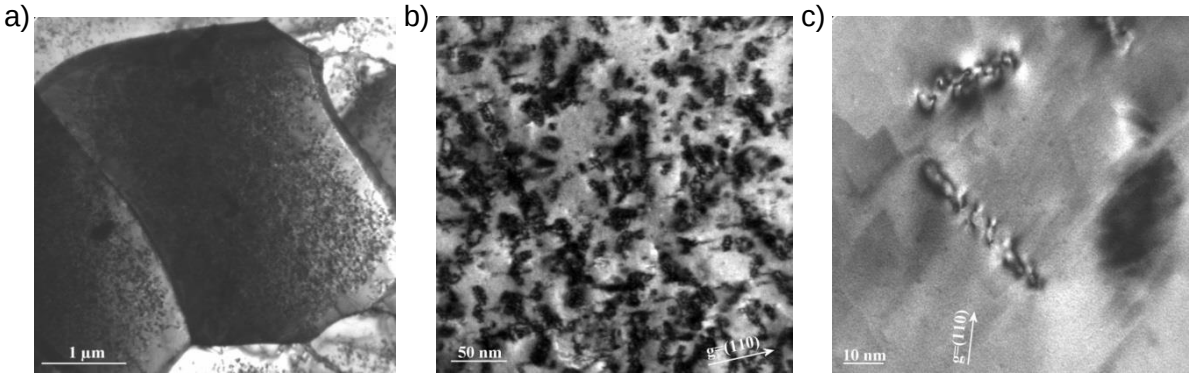

Fig. 4. a) Bright field dark field image of the grain structure in the bulk of the low dose sample, neutron irradiated to 1.47×10^{20} n/cm². b) Bright field image of the radiation induced defects. c) Higher magnification image of the convoluted dislocation loops.

In the image recorded at higher magnification, Fig. 4b and 4c, the radiation induced defects can be identified. Black dots, which are small dislocation loops, can be observed all over the grain. They were identified as a/2‹111› type loops but they are too small to be further characterized in detail. In between the loops, larger defect features were observed. They are lying on {111} type planes and they are extinct for a diffraction vector which is lying in the same {111} plane. The displacement vectors characterizing these defects are parallel to the ‹111› directions. All have the same Burgers vector and habit plane. The defect most likely corresponding to this kind of contrast is a convoluted dislocation loop [6].

Near the small-angle sub-grain boundary, a zone with a width up to 250 nm does not contain any convoluted dislocation loops. On the other hand, the small dislocation loops remain present with a concentration similar to that in the interior of the grain. The grain boundary is a strong sink for the defects which created the convoluted loops, but not for the defects creating the small dislocation loops.

The density and size of all defects were measured at a few different locations in the sample. When measuring all defects in the interior of the grain, a total defect density of 8.5×10^{21}/m³ was measured. Near the grain boundary, the concentration of the small loops can be measured. Here a density of 5×10^{21}/m³ was obtained for the small dislocation loops only.

This leaves a density of $3.5\times10^{21}/m^3$ for the convoluted dislocation loops, which agrees with the number of larger defects in the middle of the grain.

For the average size, also a distinction has to be made. When all defects are analysed, an average size of 14.8 nm was obtained. Taking, the small defects only, which are representative of the dislocation loops, an average size of 5.3 nm was measured. The convoluted dislocation loops have a much wider size range between 10 and 50 nm and the average size is 27 nm.

The formation of voids was verified in out-of-focus images, but no voids were observed at this irradiation dose.

3.3 High dose irradiated sample (4.74×10^{20} n/cm²)

The grain structure of the high dose ample is given in Fig. 5a. Similar to the sample before irradiation the grains are divided in a sub-grain structure separated by small-angle as well as large-angle grain boundaries. The size of the sub-grains is 2 µm, which is comparable to the reference material.

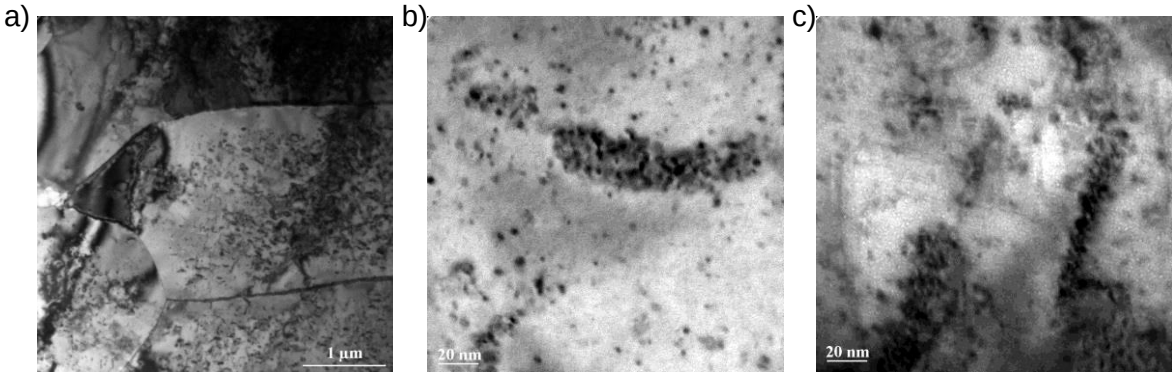

Fig. 5. a) Bright field image of the grain structure in the high dose sample. b) Bright field images of the radiation induced defects and c) under-focus image revealing voids.

Fig. 5b shows a typical bright field image of the radiation induced defects. A large amount of black dots can be observed, which can be designated as radiation induced dislocation loops. From the analysis of extinction conditions, it can be concluded that the neutron irradiation resulted in the formation of a/2‹111› type loops. The loops are too small to determine the habit plane and it cannot be concluded from this investigation whether the loops are interstitial or vacancy loops.

The loop density was measured assuming that all four linear independent a/2‹111› Burgers vectors occur equally abundant. The average density was calculated. and a defect density of $(9\pm1)\times10^{22}/m^3$ was measured. The average size of the loops, calculated from the measurement of the size of the black dot contrast, is (3.2±0.9) nm, where the precision of the measurement is a measure for the width of the size distribution.

Whereas about half of the dislocation loops are uniformly distributed over the interior of the grains or trapped at the existing line dislocations, the other half is gathered in clusters of dislocation loops. The clusters of dislocation loops were always found to be elongated indicating that they are lying on a single plane. The nature of the plane was identified as a {111} type plane. All dislocation loops show exactly the same extinction conditions, which

means that they all have the same Burgers vector. This Burgers vector is the a/2‹111› vector which is perpendicular to the {111} plane in which they are located. Similar dislocation clusters have been reported in neutron irradiated Mo [6] and Fe [7], materials which have a body centred cubic lattice like W. In these papers the alignment of the dislocation loops was referred to as raft formation. The length of the rafts ranges from 40 nm to 150 nm. The rafts are formed over the entire grain apart from the region close the low-angle and high-angle grain boundaries and there is a zone of about 100 to 200 nm which still contains the isolated dislocation loops, but not the rafts.

The formation of nanometre sized voids was verified in out-of-focus imaging conditions as in Fig. 5c. Contrary to the sample irradiated to 1.47×10^{20} n/cm², a high density of small voids could be observed in this sample. In numbers, the void density equals 2.9×10^{23}/m³, and the average size was found to be (1.0±0.2) nm, giving a volume fraction of 0.03%.

3.4 Electron beam exposed area

The effect of the electron beam exposure on the surface of the low dose and high dose samples can be observed in the SEM images of Fig. 6. Both samples were exposed to the electron beam under similar conditions. Therefore, the effect on the surface integrity is also comparable. A regular pattern of cracks was observed at the surface, which is in agreement with the expected effect for these exposure conditions [8].

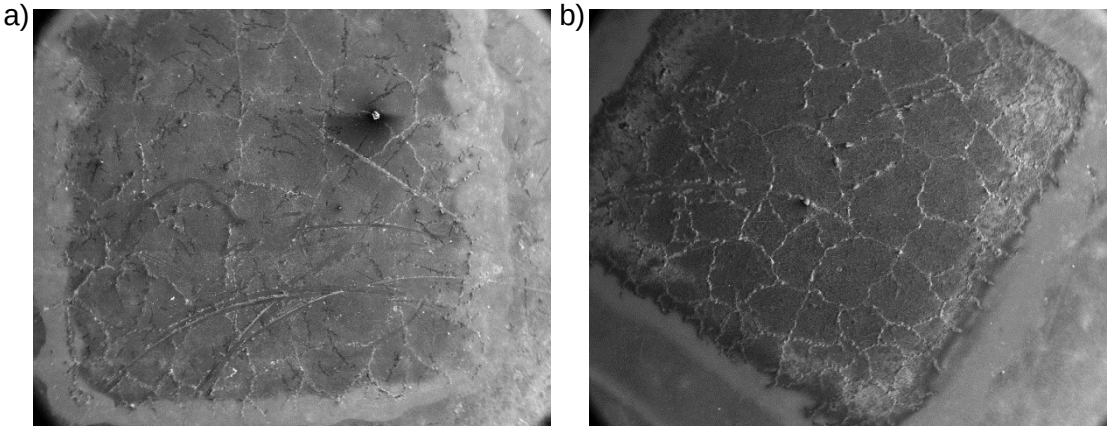

Fig. 6. Scanning electron microscopy images of the surface of neutron irradiated samples a) low dose and b) high dose after electron beam exposure.

On a microstructural level, electron beam exposure had a significant effect on the defect structure. Even though, the grain structure, as shown in Fig. 7a, is not affected by the electron beam exposure, the effect on the defects is not straight forward. In some grains, like in Fig 7b, the convoluted dislocation loops were not affected by the electron beam exposure. In other grains, all convoluted dislocation loops were removed and a network of line dislocations was formed. The formation of line dislocations results from the thermal shock during the electron beam exposure and was observed in previous experiments as well [4,5]. From extinction conditions it was determined that the majority of the line dislocations have an a/2‹111› Burgers vector, while a minority have an a‹100› Burgers vector. This result is typical for all clusters of line dislocations in all samples.

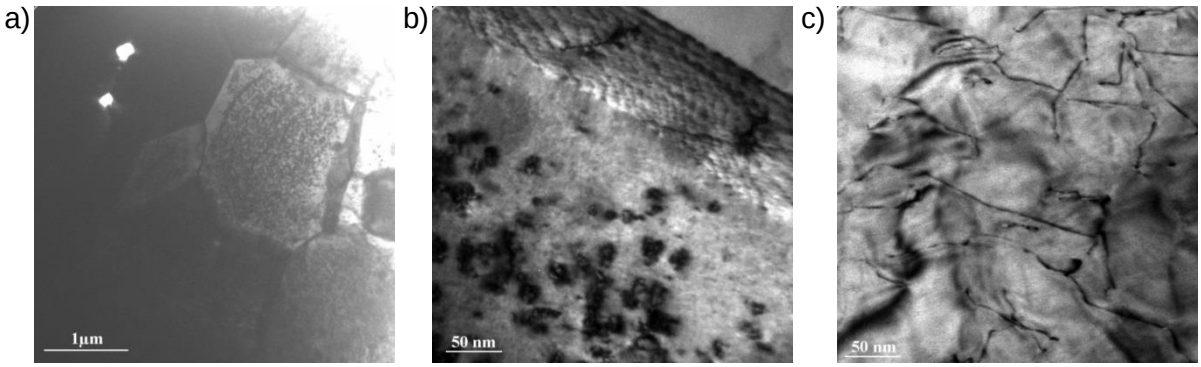

Fig. 7 a) Bright field image of the grain structure near the electron beam exposed surface of the low dose sample. b) A grain still containing convoluted dislocation loops. c) Typical defect structure in the high dose sample where almost all irradiation induced defects were removed and a dislocation network was formed.

Also in the sample irradiated to higher fluence, the electron beam exposure had no effect on the grain structure. On the other hand, the amount of line dislocations has significantly increased compared to the bulk material before and after neutron irradiation and dislocation networks are present over the entire sample. The amount of dislocation loops was drastically reduced. Contrary to the low dose sample, all dislocation rafts and almost all dislocation loops were removed in this sample.

The effect of the electron beam exposure on the voids was verified and it was found that voids are still present after the electron beam exposure. In the area the void density is 6.7×10^{22}/m³ and the average size is 1.4±0.3, giving a volume fraction of 0.02%. Compared to the values in the bulk sample, the void density is lower near the electron exposed surface, but the average size is slightly larger.

There can be two reasons for the removal of dislocation loops. Firstly, the exposed area is located close to the surface of the irradiated tungsten block. The free surface is a strong sink for mobile interstitials and vacancies, which are no longer available for loop formation. A similar effect was observed at the grain boundaries where it was found that no dislocation rafts are present. However, the effect of the free surface can explain a reduction of the total amount, but not the total disappearance of the loops. The examined area is located more than 1 µm below the surface. This is deeper than the zone denuded of rafts near a grain boundary, which was of the order of 100-200 nm. Furthermore, individual dislocation loops were still found near the grain boundaries, but not in these samples. Therefore it can be concluded that this process cannot explain the observed removal of dislocation loops.

The removal of the dislocation loops must have occurred during the dislocation network formation under the electron beam exposure. On the one hand, the line dislocations are also sinks for interstitials and vacancies and the interaction between a line dislocation and a dislocation loop can result in the annihilation of the loop. On the other hand, the temperature is locally increased, which increases the mobility of the dislocation loops, which enhances their annihilation at the free surface or the line dislocations.

4. Conclusions

Two tungsten samples obtained from a highly deformed bar were neutron irradiated in the BR2 reactor of SCK•CEN to fluences of 1.47×10^{20} n/cm² and 4.74×10^{20} n/cm² at 300°C

under a helium atmosphere and exposed to the electron beam of the Judith 1 installation to simulate the effect of a plasma disruption. The effect of these treatments on the defect structure was studied with SEM and TEM. All samples could be prepared in fume hood and a method was successfully applied to prepare the TEM samples as close to the exposed surface as possible.

The grain structure is typical for this grade of tungsten. The grains have a sub-grain structure of 1-2 µm sized grains separated mostly by low-angle grain boundaries. Only a small number of line dislocations are present mostly close to the grain boundaries. Compared to other grades of tungsten that were not re-crystallised, the orientation difference between two sub-grains is large.

The neutron irradiation created a large amount of a/2‹111› type dislocation loops. The loop density increased from $8.5\times10^{21}/m^3$ to $9\times10^{22}/m^3$ with increasing dose. The loop size decreased from 5.2 nm to 3.5 nm. This difference was mainly allocated to dislocation raft formation, where first convoluted interstitial loops are formed, which at higher irradiation dose split up in a collection of small dislocation loops.

The electron beam exposure increased the temperature near the surface to values that induced significant annealing of the defects. Almost all of the dislocation loops were removed as a result of the annealing. The number of line dislocations in that area increased as a result of the thermal shock.

5. Acknowledgement

The authors would like to thank J. Linke and G. Pintsuk of FZ Jülich for the electron beam exposure of the irradiated tungsten samples.

6. References

[1] V. Barabash, G. Federici, M. Rödig, L.L. Snead, C.H. Wu, J. Nucl. Mater. 283-287 (2000) 138-146.
[2] H. Bolt, V. Barabash, W. Krauss, J. Linke, R. Neu, S. Suzuki, N. Yoshida, ASDEX Upgrade Team, J. Nucl. Mater. 329-333 (2004) 66-73.
[3] J. Roth, E. Tsitrone, A. Loarte, Th. Loarer, G. Counsell, R. Neu et al. J. Nucl. Mater. 390-391 (2009) 1-9
[4] W. Van Renterghem, I. Uytdenhouwen, Fus. Eng. & Design 88 (2013) 1650-1654.
[5] W. Van Renterghem, I. Uytdenhouwen and Th. Loewenhoff, Proc. of 14th Int. Conf. on Plasma-Facing Materials and Components for Fusion Applications, May 13-17 (2013), Jülich, Germany, A044.
[6] K. Yamakawa and Y. Shimomura, J. Nucl. Mater. 271&272 (1999) 41-45.
[7] Zinkle S.J., Singh B.N., J. Nucl. Mater. 351 (2006) 269-284.
[8] G. Pintsuk, A. Prokhodtseva, I. Uytdenhouwen, J. Nucl. Mater 417 (2011) 481-486.